Scintillation properties of zinc tungstate-based mixed crystals

Dmitriy Matvienko*[1, 2] and Bogdan Sikach†[1]

[1]Budker institute of nuclear physics
[2]Novosibirsk state university

November 1, 2022

Abstract

Scintillation properties of several mixed crystal samples, $(Zn_{0.9}Li_{0.01}Cd_{0.1})(W_{0.9}Mo_{0.1})O_4$ and $(Zn_{0.9}Li_{0.01}Pb_{0.1})(W_{0.9}Mo_{0.1})O_4$ doped with Eu, Ce, Sc, Yt, Nb, Sm and Pr ion-activators are studied.

1 Introduction

A zinc tungstate ($ZnWO_4$) scintillation crystal is proposed for low-counting cryogenic experiments aimed to detect dark matter particles (Weakly Interacting Massive Particles, WIMP) and neutrinoless double beta decay ($0\nu2\beta$ decay). Such detection is based on signals from a low energy recoil nucleus produced by scatter of WIMP or $0\nu2\beta$ particles on nuclei. A crystal of $ZnWO_4$ has relatively high light yield at low temperatures and high intrinsic radioactive purity needed for a good detection sensitivity. Light yield can be further increased in the mixed crystals relative to the yield in their components.

In this work we consider two subsets of mixed crystals, $(Zn_{0.9}Li_{0.01}Cd_{0.1})(W_{0.9}Mo_{0.1})O_4$ ($ZnCdWO_4$) and $(Zn_{0.9}Li_{0.01}Pb_{0.1})(W_{0.9}Mo_{0.1})O_4$ ($ZnPbWO_4$), which were grown by the low-thermal-gradient Czochralski technique. The crystals are doped with various ion-activators: Eu, Ce, Sc, Yt and Nb in the $ZnCdWO_4$ subset and Eu, Sm and Pr in the $ZnPbWO_4$ subset. Considered samples can be competitive to pure $ZnWO_4$ for various applications, including low-counting scintillating detectors. The sample set consists of six cubic crystals with size of 12 mm in the $ZnCdWO_4$ subset as well as three quarter-cylinder shape crystals with an average cross section about 200 mm^2 and height 13 mm in the $ZnPbWO_4$ subset. We also have one pure $ZnWO_4$ crystal of cylindrical shape with diameter 30 mm and height 11 mm used as a reference. All samples were wrapped in two layers of 200 µm porous teflon with open bottom face.

*hoho@inp.nsk.su
†hehe@inp.nsk.su

2 Experiment

To measure the scintillation properties of the crystals the testbench shown in Fig. 1 is constructed.

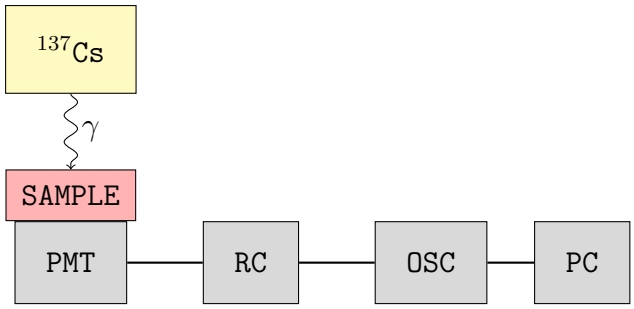

Figure 1: Testbench scheme for scintillator measurements used in the paper.

The studied sample is placed on the input window of the photomultiplier tube (PMT) Hamamtsu R1847S with optical contact Silicon Grease BC-630. The PMT R1847S has a bialkali photocathode and borosilicate glass window material, linear focused 10 stage dynode system with a typical gain of the order of 10^7 and spectral response in the range from 300 nm to 650 nm with maximum quantum efficiency of 28 % at 420 nm. The ^{137}Cs source of 662 keV photons with intensity of the order of 10^5 Bq is placed on distance of 50 mm above the top crystal face. The PMT power supply set to 1500 V is provided by the CAEN N1470 module. The PMT pulses are shaped by the RC-circuit with the time constant $\tau = 750$ ns and after that are continuously monitored by the oscilloscope OWON TDS8204 which records them to the PC memory. The internal trigger of the oscilloscope with low threshold value is applied.

3 Pulse shape analysis

All scintillation events are stored in a binary data format and processed by custom-made software based on the particle physics analysis framework ROOT. Each pulse shape is an array of 760 integer point numbers representing a signal as a function of time within a recorded length of 150 µs. Various useful parameters are calculated for individual event, such as baseline, time of trigger arrival, pulse height, time of pulse height arrival and pulse integral. Baseline is an average of event points before a trigger arrival. A pulse height is calculated as a difference between baseline and point with a largest deviation from the baseline. A pulse integral is determined as a sum of differences between baseline and event points in waveform recorded within selected time window. A typical recorded waveform from pure $ZnWO_4$ sample is demonstrated in Fig. 2. All parameters are saved in a ROOT tree structure and intensively used to create distributions under request.

4 Emission spectrum study

In order to estimate emission properties of studied mixed samples, we use the set of color glassed filters Newport FS-C, which are placed on the PMT window without optical

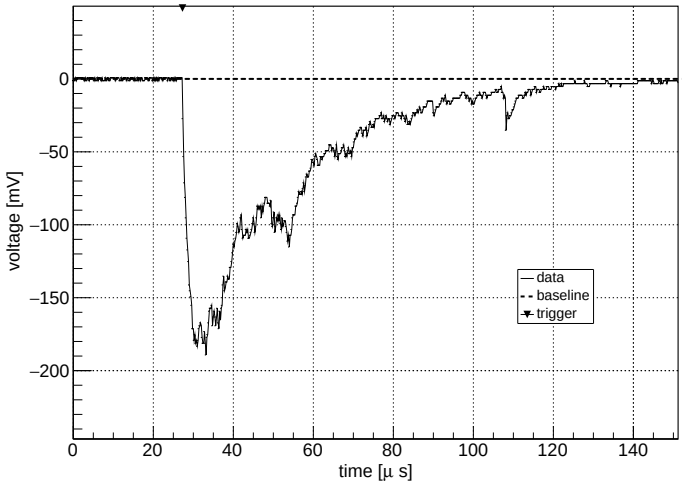

Figure 2: Typical pulse shape arrived from pure $ZnWO_4$ sample as a function of time. The solid line shows data, the dashed line demonstrates the calculated baseline level and black triangle on the top of the oscillogram corresponds to the moment of the trigger arrival.

contact. These cut-on filters have the minimum wavelengths and transmittances which are shown in Table 1.

No.	Filter model	Cut-on wavelength, nm	Transmittance
1	FSQ-GC400	400	0.90
2	FSQ-GC455	455	0.92
3	FSQ-GC515	515	0.91
4	FSQ-GC550	550	0.91
5	FSQ-GC610	610	0.93

Table 1: The set of color glassed filters used in the emission spectrum study. The cut-on wavelength and transmittance are shown.

The scintillator is put on the filter and irradiated by the α source ^{238}Pu with energy of α particles 5.1 MeV and intensity of the order of 10^5 Bq. To avoid the α particle absorption in the teflon coverage of the crystal, the small hole about 1 mm^2 is made in that.

We approximate the bandwidth $\epsilon_i(\lambda)$ of the filter No. i with the cut-on wavelength λ_i by the step function $\theta(\lambda - \lambda_i)$:

$$\epsilon_i(\lambda) = a_i\theta(\lambda - \lambda_i), \tag{1}$$

where a_i is the transmittance of the filter No. i. The fraction of photoelectron yield f_i in the range of wavelenghts between λ_i and λ_{i+1} is

$$f_i = \int_{\lambda_i}^{\lambda_{i+1}} \eta(\lambda)s(\lambda)d\lambda, \tag{2}$$

where $\eta(\lambda)$ is the PMT quantum efficiency as a function of wavelength and $s(\lambda)$ is the emission spectral function of the crystal. On the other hand, this fraction is derived using

Eq. (1) as

$$f_i = \frac{A_i/A}{a_i} - \frac{A_{i+1}/A}{a_{i+1}}, \tag{3}$$

where A_i (A_{i+1}) and A are the peak positions in the pulse integral spectrum corresponding to the filter No. i (No. $i+1$) and without filter. Suggesting the constant behaviour of the spectral function $s(\lambda) = c_i$ between two consecutive cut-on wavelengths λ_i and λ_{i+1}, we obtain from Eq. (2) that $c_i = f_i/I_i$, where f_i is calculated in Eq. (3) and $I_i = \int_{\lambda_i}^{\lambda_{i+1}} \eta(\lambda) d\lambda$.

The resulting emission spectra are shown for $ZnCdWO_4$ samples in Fig. 3. The pure

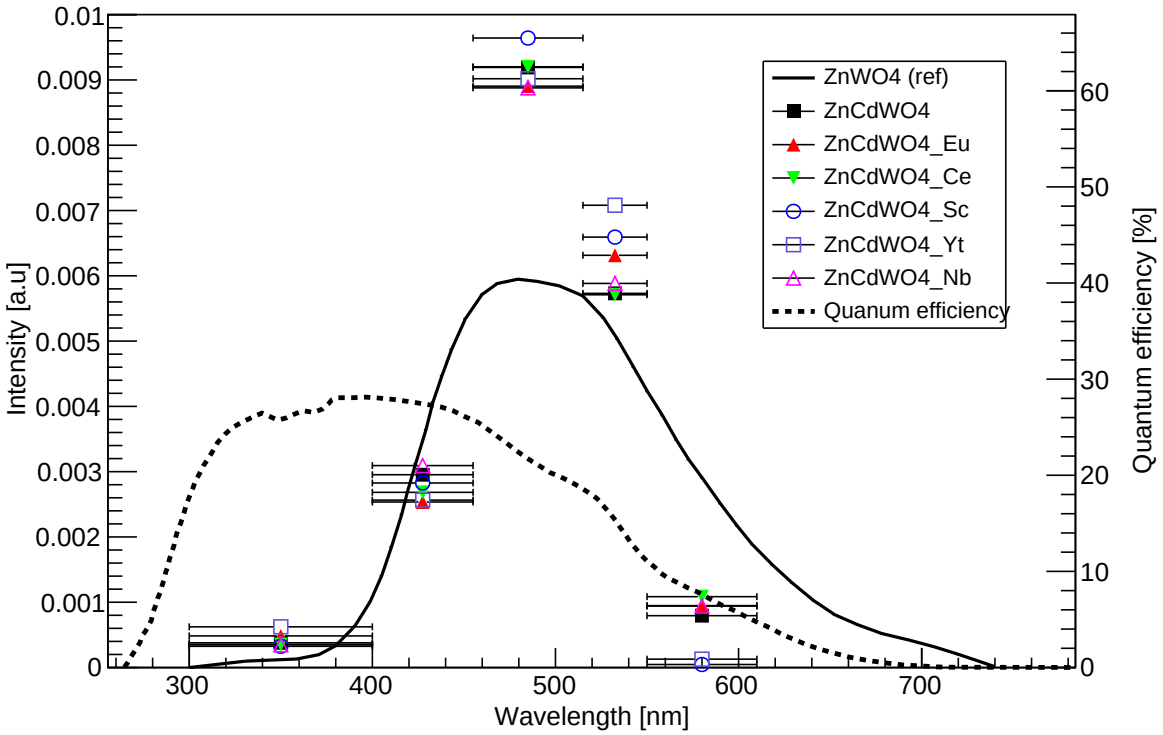

Figure 3: Emission spectra of $ZnCdWO_4$ samples. Markers show spectral sensitivities of six studied $ZnCdWO_4$ samples. The horizontal bars at the marker points are to identify the range between the cut-on wavelengths of two consecutive filters. The solid line represents the known emission spectrum of pure $ZnWO_4$. The dashed line corresponds to the PMT quantum efficiency.

$ZnWO_4$ emission spectrum taken from ref. [1] is also shown. We can see that all studied spectral spectra have a maximum intensity in a range between 460 nm and 520 nm, where the maximum intensity from the pure $ZnWO_4$ is achieved. The PMT quantum efficiency is superimposed on the plot.

The emission spectra of $ZnPbWO_4$ samples measured with the same method have very similar behavior with the $ZnCdWO_4$ spectra and shown in Fig. 4.

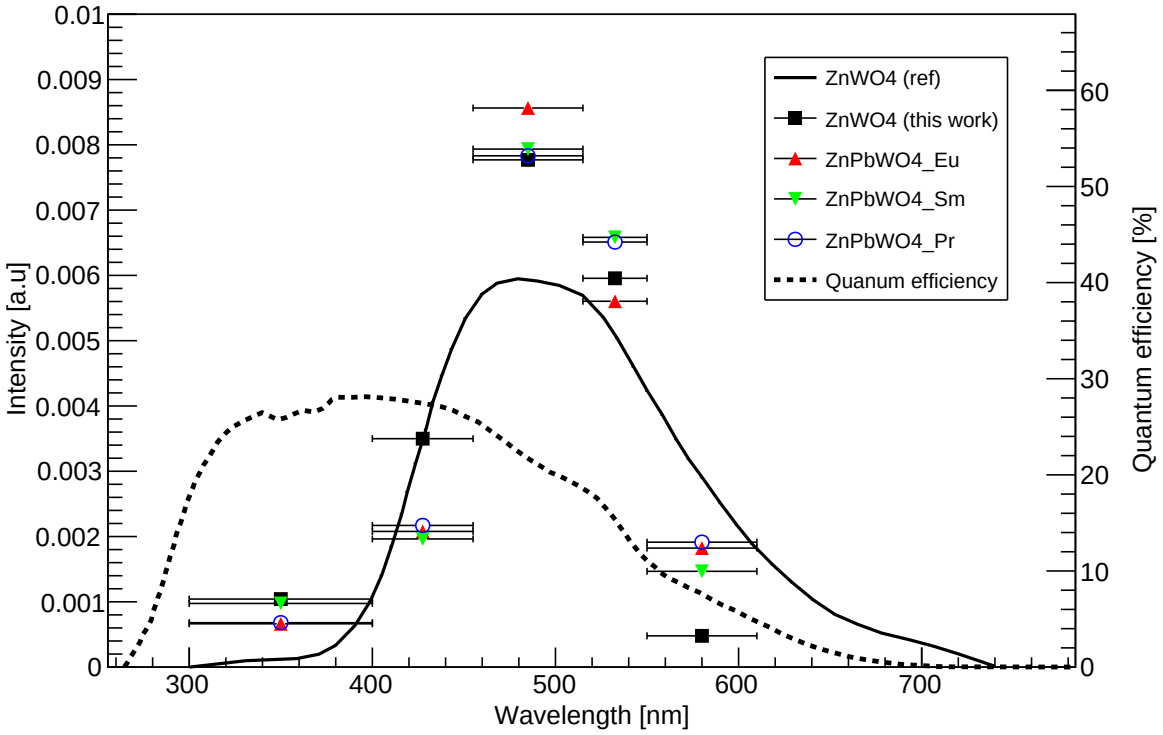

Figure 4: Emission spectra of $ZnPbWO_4$ samples. Markers show spectral sensitivities of six studied $ZnCdWO_4$ samples. The horizontal bars at the marker points are to identify the range between the cut-on wavelengths of two consecutive filters. The solid line represents the known emission spectrum of pure $ZnWO_4$. The dashed line corresponds to the PMT Hamamatsu R1847 quantum efficiency.

5 Decay time measurements

Important property of a crystal is the duration of its scintillation emission after excitation. For crystals which have more than one type of luminescent center, the time variation of the scintillation emission intensity can be described by series of exponential functions with different decay time constants.

To study the decay characteristics, we consider all the pulses in the region of the photopeak which corresponds to $\pm 2\sigma$ deviation from the mean value. An averaged pulse is constructed in this region.

Taking into account the RC time constant $\tau_{RC} = 750\,\text{ns}$ and rising time of the pulse τ_r, the average pulse is fitted by the function with two decay times τ_1 and τ_2:

$$f(t) = U_0[\alpha E(t;\tau_1) + (1-\alpha)E(t;\tau_2) - E(t;\tau_r)], \tag{4}$$

where

$$E(t;\tau_i) = \frac{\exp\{-(t-t_0)/\tau_i\} - \exp\{-(t-t_0)/\tau_{RC}\}}{1 - \dfrac{\tau_{RC}}{\tau_i}}. \tag{5}$$

Here, α is the parameter corresponding to the intensity of the component with the decay

time τ_1, t_0 is the timing shift and U_0 is the normalization constant. The shape of average pulse from the $ZnWO_4$ sample and fit by the function in Eq. (4) are shown in Fig. 5.

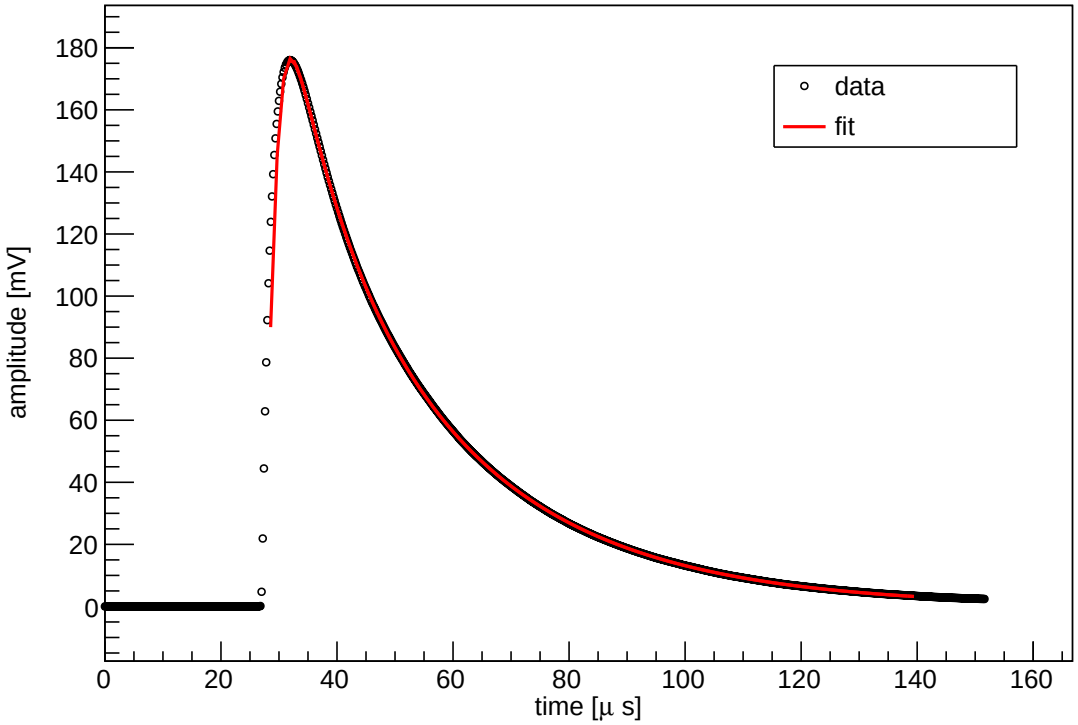

Figure 5: Average pulse shape for the $ZnWO_4$ sample. The solid curve corresponds to the fit by the function in Eq. (4).

The decay constants for two light emission components and their relative intensities for all studied samples are shown in Table 2.

Sample	τ_1 μs	α_1 %	τ_2 μs	α_2 %	Sample	τ_1 μs	α_1 %	τ_2 μs	α_2 %
$ZnWO_4$	8.2	11	27.9	89	$ZnCdWO_4 : Eu$	9.3	15	28.5	85
$ZnPbWO_4 : Eu$	12.5	24	32.0	76	$ZnCdWO_4 : Ce$	8.5	13	28.3	87
$ZnPbWO_4 : Sm$	12.6	23	32.0	77	$ZnCdWO_4 : Sc$	8.7	14	28.3	86
$ZnPbWO_4 : Pr$	13.1	26	32.5	74	$ZnCdWO_4 : Yt$	8.4	11	28.1	89
$ZnCdWO_4$	10.9	15	29.3	85	$ZnCdWO_4 : Nb$	11.3	16	29.0	84

Table 2: Decay times and their relative intensities (shown in percentage of the total intensity) of $ZnPbWO_4$ and $ZnCdWO_4$ samples.

The values of $ZnWO_4$ decay components and their intensities are in good agreement with the result obtained in [2]. We are not sensitive to the fast decay component of 0.7 µs because of limited timing resolution of 0.2 µs. The fast and slow decay components of the $ZnPbWO_4$ samples increase by 60 % and 20 %, respectively, relative to the $ZnWO_4$ scintillator. At the same time, the intensity of the fast component also increases from

10 % to 30 %. This tendency is not observable for the $ZnCdWO_4$ samples. Their decay times are comparable to the $ZnWO_4$.

All these scintillators are too slow for beam colliding experiments, where high rates are required. Nevertheless, they are potential material candidates for low-counting cryogenic experiments.

6 Light collection efficiency

Our treatment of light collection efficiencies for studied samples is based on Monte Carlo simulation with the GEANT4 package (v.10.4) and the experimental ratio $R_{\rm pe}$ (see below) between numbers of detected photons with the optical contact and without it.

The experimental setup used in the simulation is shown in Fig. 6. The dimensions of the crystals and the PMT input window match their original values in the experiment.

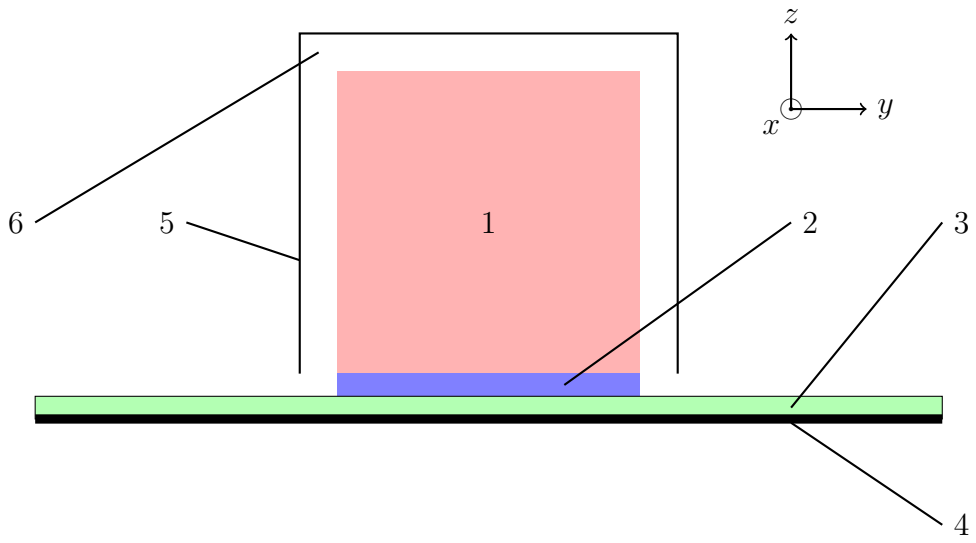

Figure 6: (color online). Schematics of the experimental setup used in the simulation (1 — crystal, 2 (blue) — gap between crystal and input window of PMT (grease or air), 3 (green) — input window of PMT, 4 (black) — photocathode of PMT, 5 — teflon wrapper, 6 — air gap between teflon wrapper and crystal surface)

The optical properties of each medium are supposed to be isotropic and its refractive index (along with the refractive index of a sample) is taken at the emission maximum of $ZnWO_4$. The full list of parameters used in the simulation is presented in Table 3.

Parameter	Comment	Value	Unit
Crystal			
Emission spectrum	@emission max	2.58 (480)	eV (nm)
Index of refraction	@emission max	2.32	-
Absorption length (γ)	$E_\gamma = 662$ keV	14.47	mm
Absorption length	@emission max	24	cm
Surface	The UNIFIED model	$C_{\mathrm{ss}}^{(\mathrm{top})}$: varies $\sigma_\alpha^{(\mathrm{top})} = 0.05$ $C_{\mathrm{ss}}^{(\mathrm{side})}$: varies $\sigma_\alpha^{(\mathrm{side})} = 0.5$	- rad - rad
Teflon wrapper			
Reflectivity	-	98	%
Gap	Size of the gap between the wrapper and crystal surface	0.1	mm
Surface parameters	The UNIFIED model used (100% diffuse reflection)	$C_{\mathrm{ss}} = 0 \quad (C_{\mathrm{dl}} = 1)$	-
Grease			
Product name	-	BC-630	-
Index of refraction	@emission max	1.465	-
Thickness	Size of the gap between bottom face of a crystal and the input window of PMT	0.1	mm
PMT input window			
Index of refraction	@emission max	1.510	-
Radius	-	26	mm
Thickness	-	1	mm
PMT photocathode			
Absorption length	If a photon reaches the photocathode it is considered to be detected	0	mm
Radius	The same as window's one	26	mm
Air			
Index of refraction	-	1.000	-

Table 3: Parameters used in the simulation.

The crucial property the light collection efficiency depends on is the finish of the surface of crystal's faces. The side and top faces of the studied samples look opaque so they perform the diffuse reflection. To take it into account the UNIFIED model (described in [**?**]) is used when constructing those faces in the simulation. The original UNIFIED model controls the radiant intensity of a surface by the four constants: C_{dl} (diffuse lobe),

$C_{\rm ss}$ (specular spike), $C_{\rm sl}$ (specular lobe) and $C_{\rm bs}$ (back-scattering). However, in this work only two of them are used (see below): $C_{\rm dl}$ and $C_{\rm ss}$. Here is a brief explanation how a photon is transported in the simulation (see Fig. 7). Suppose a photon strikes the interface between crystal and surrounding medium with the mean normal $\hat{\mathbf{n}}$ at the angle of incidence θ_i at point $\mathbf{P}$. Then the following algorithm is executed:

1. The microfacet normal $\hat{\mathbf{n}}'$ at $\mathbf{P}$ is generated so the angle α between $\hat{\mathbf{n}}$ and $\hat{\mathbf{n}}'$ is distributed according to the gaussian distribution with mean 0° and standard deviation σ_α. The azimuthal angle (not shown in Fig. 7) between the projection of the microfacet normal $\hat{\mathbf{n}}'$ onto the mean surface and the plane of incidence is sampled from the uniform distribution in the range $[0, 2\pi]$

2. The Fresnel equations are used to decide if the photon is reflected or refracted at the microfacet. At this stage the following parameters are used: the incidence angle θ_i' with respect to the microfacet normal $\hat{\mathbf{n}}'$, the refractive indices n_1, n_2 of the media and the polarization of the photon

3. If Step.2 results in reflection then either of two events are possible

   (a) Specular reflection about the mean normal $\hat{\mathbf{n}}$ with the probability of $C_{\rm ss}$

   (b) Diffuse reflection about the mean normal $\hat{\mathbf{n}}$ with the probability of $C_{\rm dl} = 1 - C_{\rm ss}$

4. If Step.2 results in refraction then the photon is refracted with the angle of refraction θ_t' about the microfacet normal $\hat{\mathbf{n}}'$ using the Snell's law

Algorithm 1: Transportation of an optical photon at the diffuse crystal surface used in the simulation

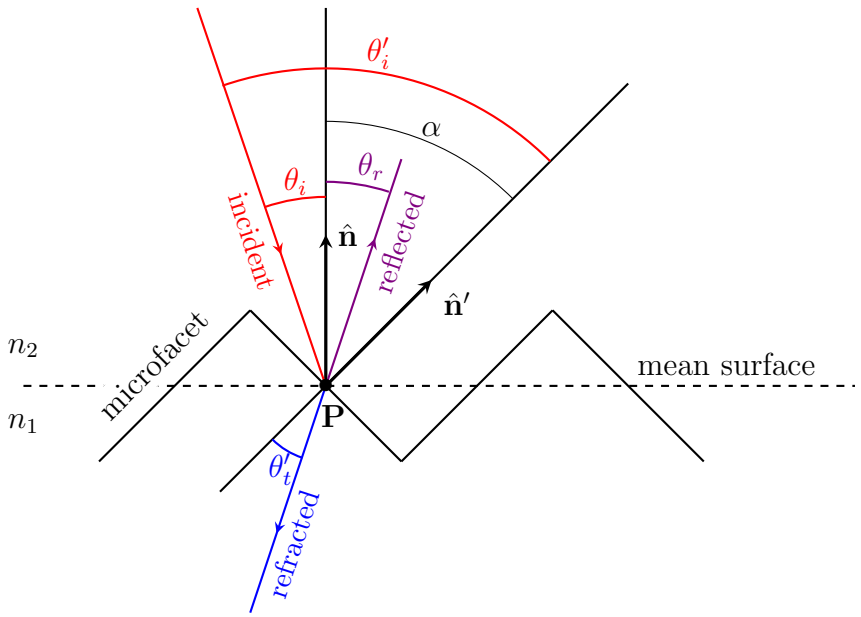

Figure 7: To the reflection and refraction processes at the diffuse crystal surface.

In short, Algorithm 1 does the following: provided a linearly polarized optical photon with a given direction meets the opaque surface of crystal a microfacet is generated.

Using the microfacet orientation and the parameters of the photon the Fresnel equations are applied to calculate the probabilities of reflection and refraction. In case of refraction, the photon is refracted *about the microfacet normal* $\hat{\mathbf{n}}'$ according to the Snell's law. In case of reflection, microfacets don't matter — either specular or diffuse reflection *about the mean normal* $\hat{\mathbf{n}}$ occurs.

The side faces differ from the top face for all samples, but the side faces themselves are considered to be identical for an individual sample. Therefore, the following set of parameters defines the surface of an individual sample in the simulation:

$$\left\{C_{\text{ss}}^{(\text{top})}, \sigma_{\alpha}^{(\text{top})}, C_{\text{ss}}^{(\text{side})}, \sigma_{\alpha}^{(\text{side})}\right\}, \tag{6}$$

where

$C_{\text{ss}}^{(\text{top})}$ — the probability of specular reflections about the average normal ($\hat{\mathbf{n}}$ in Fig. 7) of the *top* face of a sample

$\sigma_{\alpha}^{(\text{top})}$ — standard deviation of gaussian distribution according to which the microfacet normals are distributed on the *top* face of a sample

$C_{\text{ss}}^{(\text{side})}$ — the probability of specular reflections about the average normal ($\hat{\mathbf{n}}$ in Fig. 7) of the *side* faces of a sample

$\sigma_{\alpha}^{(\text{side})}$ — standard deviation of gaussian distribution according to which the microfacet normals are distributed on the *side* faces of a sample

The bottom face (in a contact with the PMT intput window) is taken 100% specular for all samples.

To estimate the surface parameters (6) we measure the energy spectrum of a sample in two different conditions: with and without optical contact between the bottom face of a crystal and the input window of PMT and then use the following parameter:

$$R_{\text{pe}} = \frac{L^{(\text{GR})}}{L^{(0)}}, \tag{7}$$

where $L^{(\text{GR})}$ and $L^{(0)}$ are positions of the photopeaks with and without optical contact, respectively. Then the values are set in such a way to make the ratio R_{pe} in the simulation to be the same as in the experiment. The side faces of all samples are very roughened so the standard deviation $\sigma_{\text{mf}}^{(\text{side})}$ is set to 0.5 rad for all samples. Instead, the top face of all samples looks more transparent than opaque so for it $\sigma_{\text{mf}}^{(\text{top})}$ is fixed at the value of 0.05 rad. Thus, the only parameters which vary from sample to sample are the probabilities $C_{\text{ss}}^{(\text{top})}$ and $C_{\text{ss}}^{(\text{side})}$ of the specular reflection at the top and side faces, respectively (see Step. 3 in Algorithm 1).

The value of the light collection efficiency in the simulation is determined as the fraction of the photons detected in the photocathode. This number varies slightly from run to run so it was averaged over 100 runs. A run consists of 10^4 transports of optical photons generated within the crystal volume. The initial point of a photon is generated according to the uniform distribution in the xy plane (parallel to the input window of PMT); and the exponential distribution along the z-axis (the axis passed through the center of a crystal and the point where the ^{137}Cs source is placed (see.Fig. 6)) with

the attenuation coefficient corresponding to the absorption length of γ-ray in $ZnWO_4$ (14.47 mm). The direction of a photon is sampled from the isotropic distribution. The polarization of a photon is a random vector perpendicular to its (photon's) direction.

The results of the simulation are summarized in Table 4. These results are in close agreement with the simulation results obtained in refs. [4] and [5].

Sample	Shape	R_{pe}	ε_{L}	Sample	Shape	R_{pe}	ε_{L}
$ZnWO_4$	cylinder	2.24	0.54	$ZnCdWO_4$:Eu	cube	1.76	0.62
$ZnPbWO_4$:Pr	quarter cylinder	1.74	0.54	$ZnCdWO_4$:Ce	cube	1.80	0.62
$ZnPbWO_4$:Eu	quarter cylinder	1.91	0.52	$ZnCdWO_4$:Sc	cube	1.78	0.62
$ZnPbWO_4$:Sm	quarter cylinder	1.91	0.52	$ZnCdWO_4$:Yt	cube	1.86	0.62
$ZnCdWO_4$	cube	2.02	0.59	$ZnCdWO_4$:Nb	cube	1.74	0.62

Table 4: The light collection efficiencies of the studied samples obtained in the simulation

7 Light yield estimation

The light yield N_{ph} per 1 MeV of energy absorbed in the scintillator can be derived as

$$N_{\mathrm{ph}} = \frac{N_{\mathrm{pe}}}{\epsilon_L \eta E_\gamma} \left[\frac{1}{\mathrm{MeV}}\right], \tag{8}$$

where N_{pe} is the number of photoelectrons produced by the scintillator in the PMT, ϵ_L is the light collection efficiency of the scintillator, η is the PMT quantum efficiency averaged by the scintillator emission spectrum and $E_\gamma = 0.662\,\mathrm{MeV}$ is the energy of photons emitted from the ^{137}Cs source. In this study the efficiency of photoelectron collection is assumed to be 100 % which is, in general, a good approximation for well-designed PMT, at least, in the central part of the photocathode.

To calibrate the PMT, we use an external light source CAEN LED driver SP5601 with tuneable intensity and output frequency. The LED driver generates ultra-fast violet color (400 nm) pulses with width of 8 ns and includes an optical fibre to simplify the light routing to the PMT input window. The light intensity is adjusted in such a way that only one or several photoelectrons per LED pulse are emitted from the photocathode and then multiply in the dynode system. The anode pulses are recorded by the OWON TDS8204 oscilloscope with external trigger provided by the LED device. The resulting integral spectrum is fitted by a sum of Gaussian functions $\sum_{i=0}^{i=4} A_i G_i(x; \mu_i, \sigma_i)$, where i represents the number of photoelectrons emitted from the cathode, $\mu_i = \mu_0 + i \times \mathrm{scale}$ and σ_i correspond to the voltage integral value on the oscilloscope and variance per i photoelectrons and A_i is the normalization coefficient. The single electron pulse spectrum and result of the fit are shown in Fig. 8. Since we calculate the baseline for each individual event, the pedestal value μ_0 is close to zero.

The photoelectron yield is obtained by comparing the single electron peak position with the scintillator photopeak position created by 662 keV photons. Calibrated integral spectra measured with the $ZnPbWO_4$ and $ZnCdWO_4$ samples are demonstrated in Fig. 9 and Fig. 10, respectively.

The clear photopeak is seen in all spectra. The back-scattered Compton peak is enhanced due to the material surrounding the ^{137}Cs source.

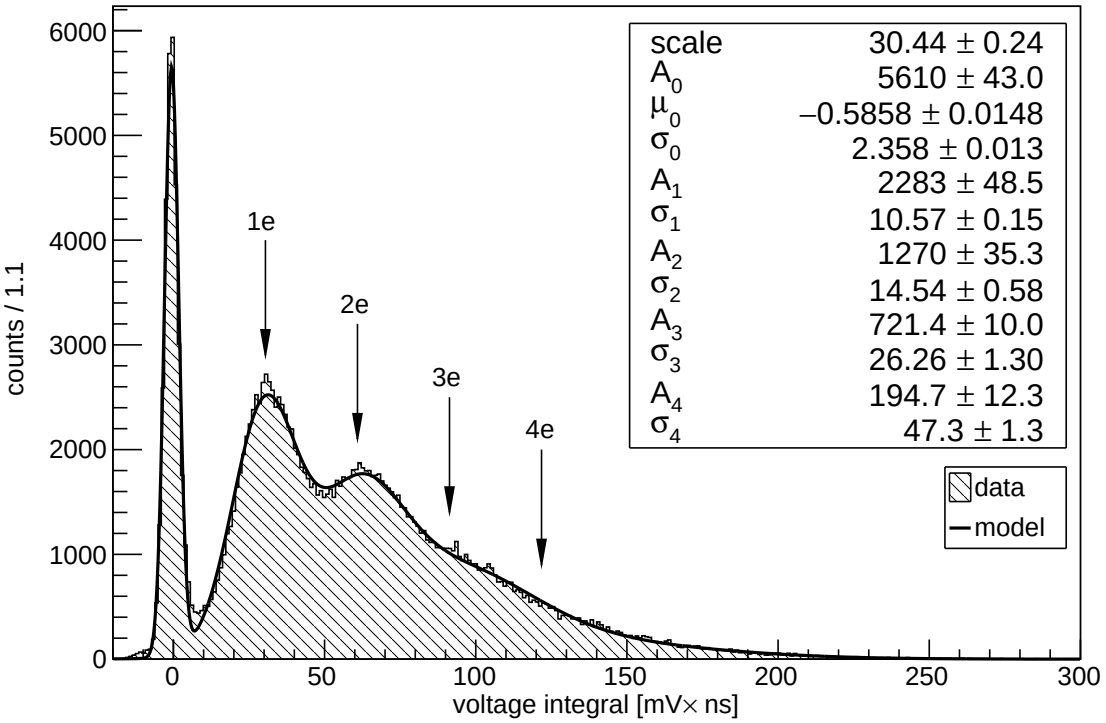

Figure 8: Single photoelectron spectrum measured with a PMT Hamamatsu R1847S.

The relative energy resolution $\Delta E/E$ is calculated as full width at half maximum (FWHM) for 662 keV photons peak divided by the number of photoelectrons. The total resolution can be written as:

$$(\Delta E/E)^2 \;=\; (\delta_{\rm sc})^2 + (\delta_{\rm st})^2, \tag{9}$$

where $\delta_{\rm sc}$ is the scintillator resolution and $\delta_{\rm st}$ is the statistical contribution related to the variation of the number of photoelectrons produced at the photocathode. The scintillator resolution includes the intrinsic resolution of the crystal and transfer resolution. The intrinsic resolution is a property of the crystal itself. It is related to non-proportionality of scintillation response, when the secondary electronic excitations at various energies deteriorate the energy resolution, and inhomogeneity of the crystal causing local variations in the scintillation light yield. Transfer resolution associates with the variation of light and photoelectron collection. The statistical resolution is described by the well-known Poisson law:

$$\delta_{\rm st} = 2.35\sqrt{\frac{1+\epsilon}{N_{\rm p.e.}}}, \tag{10}$$

where $\epsilon = 0.22$ is the variance of the PMT electron multiplier gain. The scintillator resolutions for all studied samples are shown in Table 5.

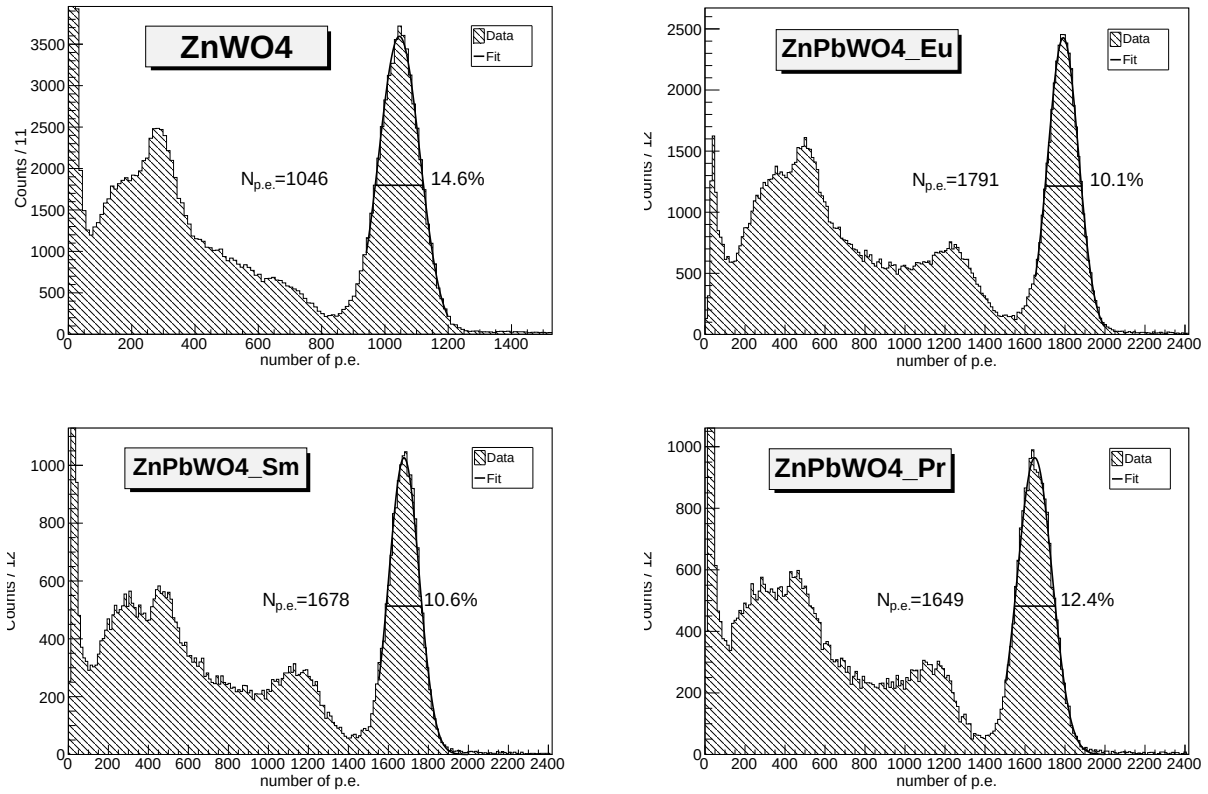

Figure 9: Pulse integral 662 keV photon spectra measured with pure $ZnWO_4$ crystal and $ZnPbWO_4$ samples. The spectra are graduated in bins of photoelectrons. The number of photoelectrons $\mu_{\text{p.e.}}$ corresponding to the 662 keV photons absorption in the scintillator and energy resolution FWHM/$\mu_{\text{p.e.}}$ are also shown.

Sample	Scintillator resolution, %	Sample	Scintillator resolution, %
$ZnWO_4$	12.2	$ZnCdWO_4 : Eu$	9.3
$ZnPbWO_4 : Eu$	8.1	$ZnCdWO_4 : Ce$	9.2
$ZnPbWO_4 : Sm$	8.5	$ZnCdWO_4 : Sc$	9.3
$ZnPbWO_4 : Pr$	10.6	$ZnCdWO_4 : Yt$	7.9
$ZnCdWO_4$	7.9	$ZnCdWO_4 : Nb$	7.8

Table 5: Scintillator resolutions for the $ZnWO_4$ crystal, $ZnPbWO_4$ and $ZnCdWO_4$ samples.

The energy resolution of $ZnWO_4$ is slightly larger than reported in refs. [6],[2],[7], which in average is 11.0 %. It can be explained in part by the crystal shape with relatively large sizes of 11×30 mm.

Taking into account emission spectra and light collection efficiencies discussed above, the absolute light yields are estimated for all samples. The photoelectron yield is integrated within the time window of 30 μsec which roughly corresponds to the main decay time constant. The results are collected in Table 6. The light yield of $ZnWO_4$ can be compared with earlier measurements of (9300 ± 570) ph/MeV with 20 µs shaping time constant obtained in ref. [8] and (7110 ± 290) ph/MeV with 12 µs shaping time presented

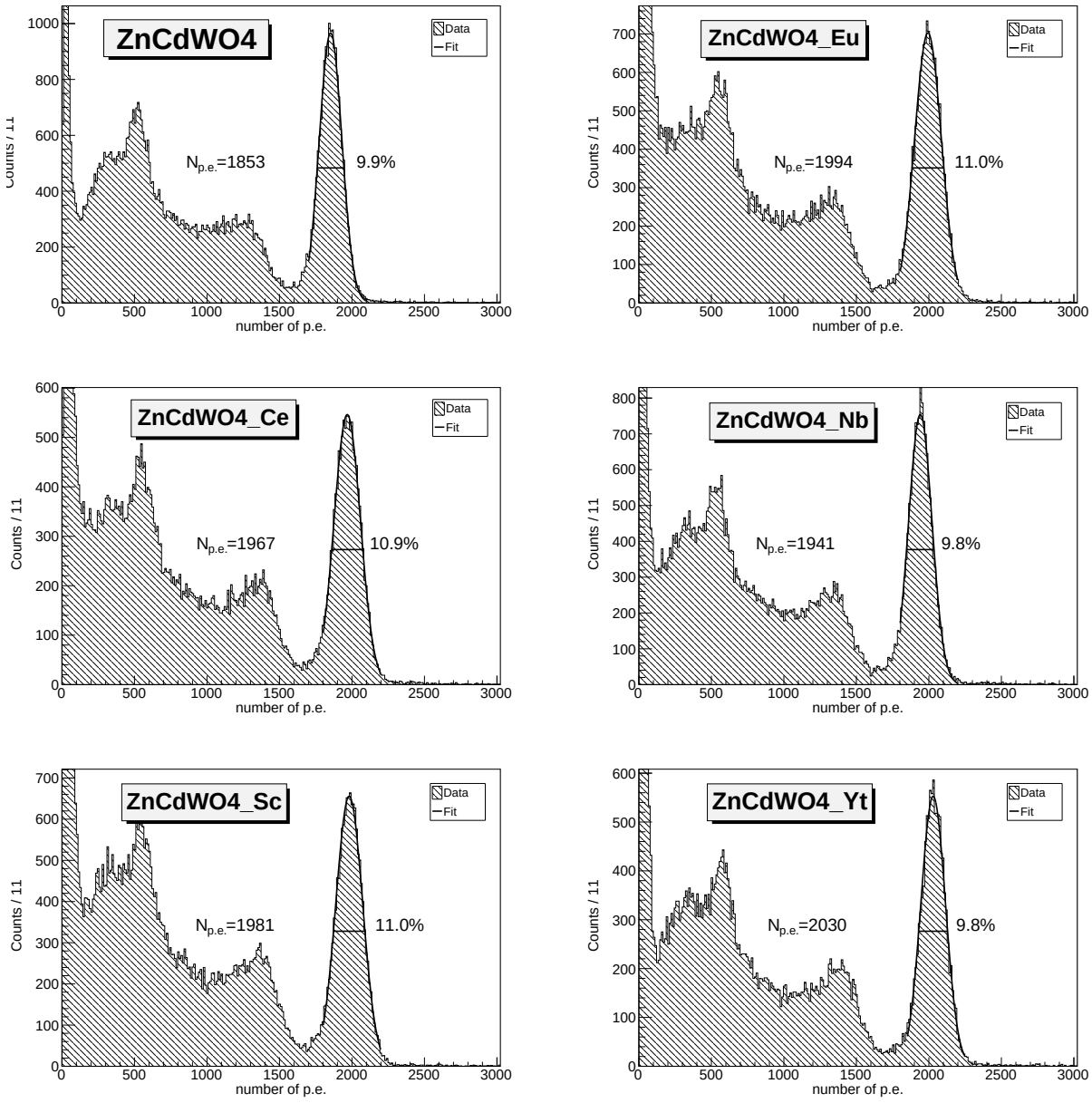

Figure 10: Pulse integral 662 keV photon spectra measured with $ZnCdWO_4$ crystals. The spectra are graduated in bins of photoelectrons. The number of photoelectrons $\mu_{\text{p.e.}}$ corresponding to the 662 keV photons absorption in the scintillator and energy resolution FWHM/$\mu_{\text{p.e.}}$ are also shown.

in ref. [7]. Recalculating the light yield within these time gates, we obtain 10 731 ph/MeV for 20 µs and 6737 ph/MeV for 12 µs. These values are in reasonable agreement with those presented in refs. [8], [7].

Sample	Time µs	Light yield ph/MeV	Sample	Time µs	Light yield ph/MeV
$ZnWO_4$	30	13 993	$ZnCdWO_4 : Eu$	30	24 134
$ZnPbWO_4 : Eu$	30	26 019	$ZnCdWO_4 : Ce$	30	22 821
$ZnPbWO_4 : Sm$	30	24 379	$ZnCdWO_4 : Sc$	30	22 519
$ZnPbWO_4 : Pr$	30	23 067	$ZnCdWO_4 : Yt$	30	22 983
$ZnCdWO_4$	30	22 591	$ZnCdWO_4 : Nb$	30	23 551

Table 6: Measured absolute light yields for the $ZnWO_4$ crystal, $ZnPbWO_4$ and $ZnCdWO_4$ samples.

8 CsI(Tl) measurement

To validate our experimental setup and pulse shape analysis, we perform measurement of the decay components and absolute light yield for well-known CsI(Tl) scintillator. To minimise effect due to the finite light collection efficiency, we select a thin sample with dimensions $10 \times 10 \times 10\,\mathrm{mm}^3$. The crystal was coated with several layers of Teflon tape and optically coupled to the PMT using BC-630 silicone grease. The crystal is irradiated by 662 keV photons from ^{137}Cs source. The PMT pulses are shaped by the RC-circuit with the time constant $\tau = 75\,\mathrm{ns}$. The time window for the integral spectrum is chosen to 3 µs. An average pulse is constructed in the region of the photopeak and fitted by the function in Eq. (4). The shape of such pulse and the fit result are shown in Fig. 11b. the decay components for the CsI(Tl) sample are shown in Table 7.

τ_1, µs	α_1, %	τ_2, µs	α_2, %
0.75	55	4.1	45

Table 7: Decay times and their relative intensities (shown in percentage of the total intensity) of the CsI(Tl) sample.

These measurements are in reasonable agreement with single photon method described in ref. [9].

Calibrated integral 662 keV photon spectrum measured with the 1 mm thick CsI(Tl) crystal is shown in Fig. 11a. To obtain the absolute photon yield, we use the reflection coefficient for the Teflon layer wrapping equal to 0.98. It results to the light yield of 65 914 ph/MeV. Scintillator resolution estimated using Eq. (9) equals to 6.6 %. We also perform an alternative measurement with 59.5 keV photons from ^{241}Am source. Taking into account the non-proportionality of the scintillation response of CsI(Tl) for photons from ^{241}Am relative to photons from ^{137}Cs described in ref. [10], the light yield is 66 106 ph/MeV, which is in a good agreement with the ^{137}Cs measurement. The light yield results for the CsI(Tl) sample are collected in Table 8.

Photon source	Light yield, ph/MeV
^{137}Cs	65 914
^{241}Am	66 106

Table 8: Light output measurement for the 1 mm thick CsI(Tl) scintillator.

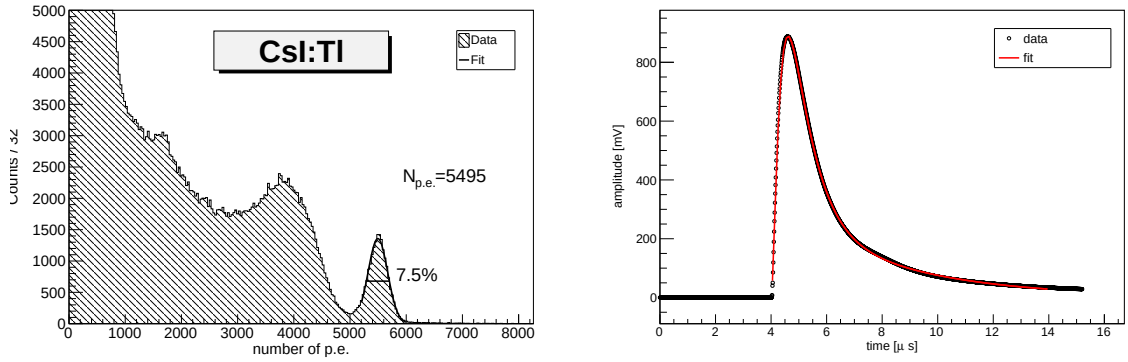

(a) (b)

Figure 11: (a) Calibrated energy spectrum of 662 keV photons from a ^{137}Cs source measured with the 1mm thick CsI(Tl) crystal and (b) average pulse shape for the CsI(Tl) sample. Points represent data, the solid line corresponds to the fit result.

Measured absolute light output of CsI(Tl) is a bit larger than in refs. [8], [11] and is close to the values obtained in refs. [12], [13].

Our sensitivity to the CsI(Tl) light yield measurement is almost full determined by systematic error in the PMT quantum efficiency curve which is extracted from manufacturer's passport and not specifically calibrated. The other main sources of systematic error are due to the knowledge of CsI(Tl) emission spectrum and quantum efficiency enhancement by multiple light reflections from the PMT photocathode.

9 Conclusion

Scintillation properties of several zinc tungstate-based mixed crystals grown with the low-thermal-gradient Czochralski technique are studied at room temperature. We have one pure $ZnWO_4$ crystal used as a reference, three $(Zn_{0.9}Li_{0.01}Pb_{0.1})(W_{0.9}Mo_{0.1})O_4$ mixed crystals doped with Eu, Sm and Pr with 0.01 mol% concentration and, finally, six $(Zn_{0.9}Li_{0.01}Cd_{0.1})(W_{0.9}Mo_{0.1})O_4$ mixed crystals, where five of them are doped with Eu, Ce, Sc, Yt, and Nb with 0.01 mol% concentration.

Analysis of their emission spectra and decay time components shows the properties similar to the pure $ZnWO_4$ crystal. However, their absolute light yields are increased by a factor of two relative to the $ZnWO_4$ scintillator. Their energy resolutions are also improved in comparison with $ZnWO_4$. All absolute light yields and scintillator resolutions are shown in Fig. 12.

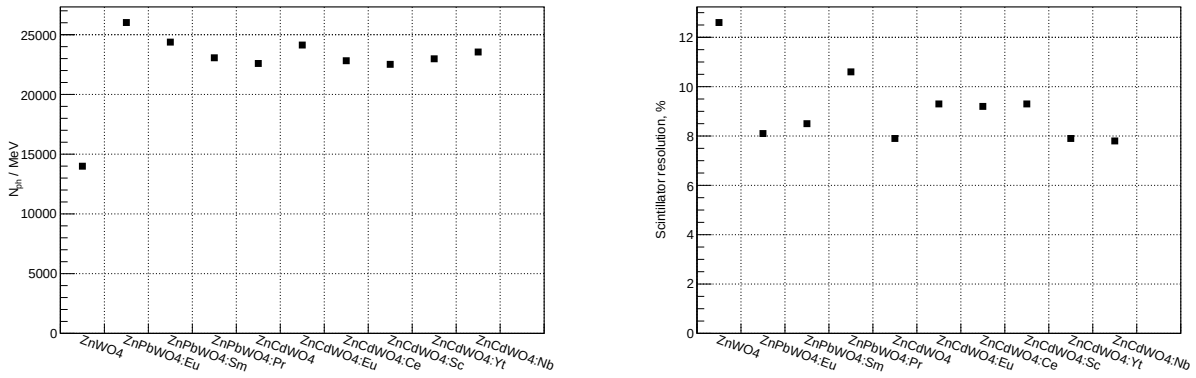

(a) (b)

Figure 12: (a) Light yields and (b) scintillator resolutions for all studied samples.

References

[1] H. Kraus, V. Mikhailik, Y. Ramachers, D. Day, K. Hutton and J. Tefler, *Feasibility study of $ZnWO_4$ scintillator for exploiting materials signature in cryogenic WIMP dark matter searches.*, Phys. Lett. B **610**, 37 (2005).

[2] F. Danevich, V. Kobychev, D. Poda and V. Tretyak, *$ZnWO_4$ as detectors for 2β decay and dark matter experiments*, Nucl. Instrum. and Meth. in Phys. Res. Sect. A **544**, 553 (2005).

[3] A. Levin and C. Moisan, *A More Physical Approach to Model the Surface Treatment of Scintillation Counters and its Implementation into DETECT*, IEEE Nuclear Science Symposium. Conference Record (1996).

[4] F. A. Danevich, V. V. Kobychev, R. V. Kobychev, H. Kraus, V. B. Mikhailik, V. M. Mokina and I. M. Solsky, *Impact of geometry on light collection efficiency of scintillation detectors for cryogenic rare event searches*, Nucl. Instrum. Meth. B **336**, 26 (2014)

[5] F. A. Danevich, R. V. Kobychev, V. V. Kobychev, H. Kraus, V. B. Mikhailik and V. M. Mokina, *Optimization of light collection from crystal scintillators for cryogenic experiments*, Nucl. Instrum. Meth. A **744**, 41 (2014)

[6] H. Kraus, F. Danevich, S. Henry, V. Kobychev *et al.*, *$ZnWO_4$ scintillators for cryogenic dark matter experiments*, Nucl. Instrum. and Meth. in Phys. Res. Sect. A **600**, 594 (2009).

[7] W. Klamra, T. Szczesniak, M. Moszynski, J. Iwanowska *et al.*, *Properties of $CdWO_4$ and $ZnWO_4$ scintillators at liquid nitrogen temperature*, Journal of Instrum. **7**, P03011 (2012).

[8] I. Holl, E. Lorenz and G. Mageras, *A measurement of the light yield of common inorganic scintillators*, IEEE Transactions of Nuclear Science, **35**, 105 (1988).

[9] A. Syntfeld and M. Moszynski, *Light pulse dependence on γ ray energy in CsI(Tl)*, IEEE Transactions of Nuclear Science, **55**, 1246 (2008).

[10] P. Dorenbos, J.T.M. de Haas and C.W.E. vasn Eijk, *Non-proportionality in the scintillation response and the energy resolution obtainable with scintillation crystals*, IEEE Transactions of Nuclear Science, **42**, 2190 (1995).

[11] E. Sakai, *Recent measurements on scintillator-photodetector systems*, IEEE Transactions of Nuclear Science, **34**, 418 (1987).

[12] M. Moszynski, M. Kapusta, M. Mayhugh, D. Wolski and S.Flyckt, *Absolute light output of scintillators*, IEEE Transactions of Nuclear Science, **44**, 1052 (1997).

[13] J. Valentine, D. Wehe, G. Knoll and C. Moss, *Temperature dependence of CsI(Tl) absolute scintillation yield*, IEEE Transactions of Nuclear Science, **40**, 1267 (1993).